AIMS Mathematics, 10(10): 23360–23379.
DOI:10.3934/math.20251037
Received: 26 August 2025
Revised: 24 September 2025
Accepted: 10 October 2025
Published: 15 October 2025

https://www.aimspress.com/journal/Math

*Research article*

# An inertial hybrid CGP-based algorithm with restart strategy for constrained nonlinear equations and impulse noise image restoration

**Yan Xia and Dandan Li***

School of Artificial Intelligence, Guangzhou Huashang College, Guangzhou 511300, China

* **Correspondence:** Email: liddjq@gdhsc.edu.cn.

**Abstract:** The conjugate gradient method is widely recognized as one of the most efficient approaches for solving large-scale optimization problems. In this paper, we have propose a novel hybrid conjugate gradient projection (CGP)-based algorithm that integrates an improved conjugate coefficient derived from the Hestenes-Stiefel (HS) and Polak-Ribière-Polak (PRP) formulas. The proposed algorithm exhibits several key characteristics: (i) The hybrid coefficient with a single parameter was employed to construct a search direction that ensures both the sufficient descent condition and trust-region feature, enhanced via a restart strategy; (ii) we incorporated an inertial-relaxed scheme alongside a projection technique in a hybrid CGP-based framework for further improving performance; (iii) we established the global convergence of the proposed algorithm under relaxed assumptions, providing a solid theoretical foundation; and (iv) extensive numerical experiments demonstrated the superior numerical performance of the proposed algorithm compared to existing algorithms on large-scale constrained nonlinear equations and impulse noise image restoration problems.

**Keywords:** nonlinear equations; conjugate gradient projection method; inertial-related scheme; theoretical analysis; impulse noise image restoration
**Mathematics Subject Classification:** 65K05, 90C56

## 1. Introduction

The goal of this paper is to find solutions of constrained nonlinear monotone equations (CNME), which can be formulated as follows:

$$G(x) = 0, \quad x \in \mathcal{D}, \tag{1.1}$$

where $G : \mathbb{R}^n \to \mathbb{R}^n$ is continuous, and $\mathcal{D} \subseteq \mathbb{R}^n$ is a non-empty and closed convex set. Specifically, the CNME (1.1) reduces to unconstrained nonlinear monotone equations when $\mathcal{D}$ is set to $\mathbb{R}^n$.

Nonlinear monotone equations have received significant attention in various engineering applications, such as compressive sensing [1,2], machine learning [3], logistic regression [4], and traffic

assignment [5]. Generally speaking, iterative methods for solving nonlinear monotone equations can be categorized into two primary types: derivative-based methods and derivative-free methods. Derivative-based methods include Newton-type methods [6, 7], quasi-Newton methods [8, 9], and Levenberg-Marquardt methods [10]. These methods are known for their rapid convergence. However, they are often difficult to apply to large-scale nonlinear equations due to the need to compute and store the Jacobian matrix or its approximation at each iteration. In contrast, derivative-free methods have proven to be well-suited for large-scale nonlinear equations, as they do not rely on derivatives, making them more efficient for such problems.

The CGP method, a derivative-free approach, is widely recognized as an efficient technique for solving large-scale nonlinear equations. This efficiency stems from its simplicity and low memory requirements. For instance, Salihu et al. [11] proposed an enhanced spectral CGP-based method for solving monotone nonlinear equations, particularly in signal processing applications. In another example, Waziri et al. [12] combined the adaptive PRP scheme with the projection technique, presenting a numerically efficient PRP-type method for systems of monotone nonlinear equations where the solution is confined to a closed convex set. Based on the three-term conjugate gradient method and hybrid techniques, Yin et al. [13] introduced a hybrid three-term CGP method, incorporating an adaptive line search for solving large-scale nonlinear monotone equations with convex constraints. Additional relevant methods can be found in works such as [14–16]. However, these approaches do not consider the integration of the inertial-relaxed scheme, which replaces the current point with an inertial point that includes both the current and previous points. This scheme is designed to accelerate the method and improve its performance. Some recent works have employed this scheme to enhance the numerical performance of the CGP method. For example, Liu et al. [17] developed a spectral CGP-based method with an inertial factor for solving nonlinear equations, while Zheng et al. [18] improved the Fletcher-Reeves (FR) conjugate parameter with a shrinkage multiplier, leading to a derivative-free two-term search direction and its extended spectral version. Further inertial-relaxed CGP-based methods can be found in [19–21].

In this paper, we focus on enhancing the double-parameter-based conjugate gradient methods introduced in [22] by utilizing a hybridization approach and a restart strategy. To achieve this, we propose an inertial hybrid CGP-based algorithm for solving the CNME (1.1) and apply it to impulse noise image restoration problems. The key contributions of this paper are outlined as follows:

♦ A hybrid conjugate coefficient with a single parameter is designed based on a double-parameter conjugate coefficient. This new conjugate coefficient is then used to construct a novel search direction that satisfies the sufficient descent property and trust region feature by integrating the restart strategy.

♦ By combining the projection technique with an inertial scheme, we propose an inertial hybrid CGP-based algorithm for solving constrained nonlinear equations and addressing impulse noise image restoration. The global convergence of the proposed algorithm is proved under weaker assumptions, which only require the monotonicity of the nonlinear equations.

♦ The proposed algorithm is applied to large-scale constrained nonlinear equations and impulse noise image restoration problems. Experimental results demonstrate its efficiency and competitiveness compared to existing methods.

## 2. Motivation and algorithm

In this section, we propose an inertial hybrid CGP-based (IHCGPB) algorithm, which is designed by introducing a new hybrid conjugate coefficient and incorporating a restart strategy to accelerate the descent of its search direction.

To begin with, we review conjugate gradient methods, which are widely used to solve unconstrained optimization problems of the form $\min\{f(x) \mid x \in \mathbb{R}^n\}$. These methods iterate along the update formula $x_{k+1} = x_k + t_k d_k$, where $t_k$ denotes the step-length, and $d_k$ is the search direction determined by the conjugate coefficient $\beta_k$. Some well-known conjugate coefficients include the FR, PRP, HS, and Dai-Yuan (DY), which are defined as follows:

$$\beta_k^{FR} = \frac{\|g_k\|^2}{\|g_{k-1}\|^2}, \quad \beta_k^{PRP} = \frac{g_k^T v_{k-1}}{\|g_{k-1}\|^2}, \quad \beta_k^{HS} = \frac{g_k^T v_{k-1}}{d_{k-1}^T v_{k-1}}, \quad \beta_k^{DY} = \frac{\|g_k\|^2}{d_{k-1}^T v_{k-1}},$$

where $g_k := \nabla f(x_k)$, $v_{k-1} = g_k - g_{k-1}$, and $\|\cdot\|$ denotes the Euclidean norm. According to these methods, Nazareth [22] proposed a hybrid formulation of a double-parameter-based conjugate coefficient, defined by

$$\beta_k = \frac{\lambda_k \|g_k\|^2 + (1-\lambda_k) g_k^T v_{k-1}}{\eta_k \|g_{k-1}\|^2 + (1-\eta_k) d_{k-1}^T v_{k-1}}, \tag{2.1}$$

where $0 \le \lambda_k, \eta_k \le 1$. To ensure the sufficient descent condition, Wei et al. [23] slightly modified the HS method, yielding a new conjugate coefficient formula:

$$\beta_k = \frac{g_k^T \left( g_k - \frac{g_k^T g_{k-1}}{\|g_{k-1}\|^2} g_{k-1} \right)}{d_{k-1}^T v_{k-1}}. \tag{2.2}$$

Similarly, Zhang et al. [24] proposed a modified PRP conjugate gradient method, which introduced a new formula for the conjugate coefficient:

$$\beta_k = \frac{g_k^T \left( g_k - \frac{g_k^T g_{k-1}}{\|g_{k-1}\|^2} g_{k-1} \right)}{\|g_{k-1}\|^2}. \tag{2.3}$$

Motivated by the construction of the hybrid conjugate coefficient defined in (2.1), and inspired by the improvements made to the HS and PRP conjugate coefficients defined in (2.2) and (2.3), we propose a new double-parameter-based conjugate coefficient. This coefficient is designed to enhance the theoretical and numerical performance. Specifically, it is expressed as:

$$\beta_k = \frac{\lambda_k \left[ g_k^T \left( g_k - \frac{g_k^T g_{k-1}}{\|g_{k-1}\|^2} g_{k-1} \right) \right] + (1-\lambda_k) \|g_k\|^2}{\eta_k \|g_{k-1}\|^2 + (1-\eta_k) d_{k-1}^T v_{k-1}}, \tag{2.4}$$

which allows the method to incorporate information from each of the four methods at every iteration. However, the selection of the double parameters (i.e., $\lambda_k$ and $\eta_k$) is not trivial. By setting $\eta_k = \frac{1}{2}$, we can simplify (2.4) into a single-parameter-based conjugate coefficient as follows:

$$\beta_k = \frac{2 \left( \|g_k\|^2 - \lambda_k \frac{\left(g_k^T g_{k-1}\right)^2}{\|g_{k-1}\|^2} \right)}{\|g_{k-1}\|^2 + d_{k-1}^T v_{k-1}}, \tag{2.5}$$

which serves as a more tractable alternative. To ensure the global convergence under weaker assumptions, we further refine this expression to:

$$\beta_k = \frac{2\left(\|g_k\|^2 - \lambda_k \frac{\left(g_k^T g_{k-1}\right)^2}{\|g_{k-1}\|^2}\right)}{\max\left\{\|g_{k-1}\|^2 + d_{k-1}^T v_{k-1}, \mu_1\|g_{k-1}\|^2, \mu_2\|g_k\|\|d_{k-1}\|\right\}}, \tag{2.6}$$

where $\mu_1 \geq 2$ and $\mu_2 > 0$. Based on the above discussion, we propose an inertial hybrid CGP-based algorithm with a restart strategy to solve the CNME (1.1) by extending this conjugate coefficient (2.6). The inertial scheme of such an algorithm is used to evaluate the inertial step-length through the following formula:

$$\tau_k = \begin{cases} \min\left\{\tau, \frac{1}{k^2\|x_k - x_{k-1}\|^2}\right\}, & \text{if } x_k \neq x_{k-1}, \\ \tau, & \text{otherwise}, \end{cases} \tag{2.7}$$

where $\tau \in (0, 1)$ and $0 \leq \tau_k \leq \tau < 1$. From this, the following inequality holds:

$$\tau_k\|x_k - x_{k-1}\|^2 \leq \frac{1}{k^2}, \quad \forall k \geq 1, \tag{2.8}$$

which implies that:

$$\sum_{k=1}^{+\infty} \tau_k\|x_k - x_{k-1}\|^2 \leq \sum_{k=1}^{+\infty} \frac{1}{k^2} < +\infty. \tag{2.9}$$

Using this inertial step-length, we evaluate the inertial point by $y_k = x_k + \tau_k(x_k - x_{k-1})$. Consequently, the search direction is defined as:

$$d_k = \begin{cases} -G(y_k), & k = 0, \\ -G(y_k) + \beta_k^{IHCGP} d_{k-1}, & \text{if flag and } k \geq 1, \\ -G(y_k) + \zeta \frac{G(y_k)^T d_{k-1}}{\|d_{k-1}\|^2} d_{k-1}, & \text{otherwise}, \end{cases} \tag{2.10}$$

where

$$\text{flag} := -\upsilon_1\|G(y_{k-1})\|^2 \leq G(y_k)^T d_{k-1} \leq \upsilon_2\|G(y_{k-1})\|^2 \in \{\text{True}, \text{False}\},$$

$$\beta_k^{IHCGP} = \frac{2\left(\|G(y_k)\|^2 - \lambda_k \frac{\left(G(y_k)^T G(y_{k-1})\right)^2}{\|G(y_{k-1})\|^2}\right)}{\max\left\{\|G(y_{k-1})\|^2 + d_{k-1}^T \tilde{v}_{k-1}, \mu_1\|G(y_{k-1})\|^2, \mu_2\|G(y_k)\|\|d_{k-1}\|\right\}}, \tag{2.11}$$

and $|\zeta| < 1$, $\tilde{v}_{k-1} = G(y_k) - G(y_{k-1})$, $0 < \upsilon_1, \upsilon_2 < 1$.

Based on the search direction in (2.10) and the conjugate coefficient in (2.11), we describe the proposed algorithm as follows:

**Algorithm 1** IHCGPB algorithm

**Step 0.** Initial points $x_0 \in \mathbb{R}^n$; Parameters $\epsilon \in (0,1)$, $\mu_1 \geq 2$, $\mu_2 > 0$, $\tau \in (0,1)$, $\varsigma > 0$, $\rho \in (0,1)$, $\sigma > 0$, $\kappa_2 > \kappa_1 > 0$, $0 < \upsilon_1, \upsilon_2 < 1$, $0 < \lambda_k < 1$, and $\gamma \in (0,2)$; Set $k := 0$ and $x_{-1} := x_0$.

**Step 1.** Evaluate $\|G(x_k)\|$. If $\|G(x_k)\| \leq \epsilon$, then stop.

**Step 2.** Evaluate the inertial step-length by (2.7) to generate $y_k = x_k + \tau_k(x_k - x_{k-1})$. If $\|G(y_k)\| \leq \epsilon$, then stop.

**Step 3.** Evaluate the search direction $d_k$ by (2.10) and (2.11).

**Step 4.** Set $z_k = y_k + t_k d_k$, where the step-length $t_k = \varsigma\rho^{i_k}$ and $i_k$ is the smallest non-negative integer $i$ that satisfies

$$-G(y_k + \varsigma\rho^i d_k)^T d_k \geq \sigma\varsigma\rho^i M_k(i)\|d_k\|^2, \tag{2.12}$$

where $M_k(i) = \min\left\{\kappa_2, \max\left\{\|G(y_k + \varsigma\rho^i d_k)\|, \kappa_1\right\}\right\}$. If $\|G(z_k)\| \leq \epsilon$, then stop.

**Step 5.** Evaluate the next point $x_{k+1}$ by

$$x_{k+1} = \mathcal{P}_{\mathcal{D}}\left[y_k - \gamma\vartheta_k G(z_k)\right], \quad \vartheta_k = \frac{G(z_k)^T(y_k - z_k)}{\|G(z_k)\|^2}. \tag{2.13}$$

**Remark 1.** *The adaptive line search approach in* (2.12) *is well-defined, and its complete proof can be found in Lemma 3.2 of [25]. This implies that there exists a positive integer $i_k$ such that* (2.12) *holds. Otherwise, we assume that there exists an index $k_0 \geq 0$ such that* (2.12) *is not satisfied for any i, i.e.,*

$$-G(y_{k_0} + \varsigma\rho^i d_{k_0})^T d_{k_0} < \sigma\varsigma\rho^i M_{k_0}(i)\|d_{k_0}\|^2.$$

*We take limits in this inequality as $i \to +\infty$, which indicates that $G(y_{k_0})^T d_{k_0} \geq 0$ is satisfied from the continuity of $G$ and $\rho \in (0,1)$. However, this result contradicts the sufficient descent property discussed in Section 3. Therefore, the adaptive line search approach is well-defined.*

**Remark 2.** *From Step 5 of the IHCGPB algorithm, for the closed convex set $\mathcal{D} \subseteq \mathbb{R}^n$, the projection operator $\mathcal{P}_{\mathcal{D}}[\cdot]$ is defined as:*

$$\mathcal{P}_{\mathcal{D}}[x] = \arg\min\{\|y - x\| \mid y \in \mathcal{D}\}.$$

*This projection operator satisfies the non-expensive property:*

$$\|\mathcal{P}_{\mathcal{D}}[x] - \mathcal{P}_{\mathcal{D}}[y]\| \leq \|x - y\|, \quad \forall x, y \in \mathbb{R}^n. \tag{2.14}$$

## 3. Theoretical analysis of the proposed algorithm

In this section, we present the theoretical analysis of the IHCGPB algorithm. To facilitate this analysis, we introduce the following general assumptions:

**Assumption A1:** The CNME (1.1) has a non-empty solution set $\mathcal{D}_*$.

**Assumption A2:** The function $G(x)$ is monotone over the set $\mathbb{R}^n$, i.e.,

$$(G(x) - G(y))^T (x - y) \geq 0, \quad \forall x, y \in \mathbb{R}^n.$$

These assumptions are fundamental in establishing the convergence behavior of the IHCGPB algorithm, as they ensure that the iterative process converges to a solution within the feasible region of the CNME (1.1).

The following lemma shows that the search direction generated by the algorithm satisfies the sufficient descent property.

**Lemma 1.** *For all $k \geq 0$, the search direction generated from* (2.10) *and* (2.11) *satisfies the sufficient descent property, i.e.,*

$$G(y_k)^T d_k \leq -N\|G(y_k)\|^2, \tag{3.1}$$

*where $N = \min\{1 - \frac{2\upsilon}{\mu_1}, 1 - \zeta\}$ and $\upsilon = \max\{\upsilon_1, \upsilon_2\}$.*

*Proof.* For $k = 0$, it is easy to observe that $G(y_0)^T d_0 = -\|G(y_0)\|^2$. For $k \geq 0$, we proceed by considering the following two cases:

(i) If $-\upsilon_1\|G(y_{k-1})\|^2 \leq G(y_k)^T d_{k-1} \leq \upsilon_2\|G(y_{k-1})\|^2$, then the relation $\left|G(y_k)^T d_{k-1}\right| \leq \upsilon\|G(y_{k-1})\|^2$ holds, with $\upsilon = \max\{\upsilon_1, \upsilon_2\}$. Combining this with (2.10) and (2.11), we derive the following inequality:

$$\begin{aligned} G(y_k)^T d_k &= -\|G(y_k)\|^2 + \beta_k^{IHCGP} G(y_k)^T d_{k-1} \\ &\leq -\|G(y_k)\|^2 + \beta_k^{IHCGP} \left|G(y_k)^T d_{k-1}\right| \\ &\leq -\|G(y_k)\|^2 + \frac{2\|G(y_k)\|^2}{\mu_1\|G(y_{k-1})\|^2}\upsilon\|G(y_{k-1})\|^2 \\ &= -\left(1 - \frac{2\upsilon}{\mu_1}\right)\|G(y_k)\|^2. \end{aligned}$$

(ii) If $G(y_k)^T d_{k-1} < -\upsilon_1\|G(y_{k-1})\|^2$ or $G(y_k)^T d_{k-1} > \upsilon_2\|G(y_{k-1})\|^2$, then the following relation holds:

$$G(y_k)^T d_k \leq -\|G(y_k)\|^2 + \zeta\frac{\|G(y_k)\|\|d_{k-1}\|}{\|d_{k-1}\|^2}\|G(y_k)\|\|d_{k-1}\| = -(1-\zeta)\|G(y_k)\|^2.$$

By combining the results from these two cases, we conclude that $G(y_k)^T d_k \leq N\|G(y_k)\|^2$ with $N = \min\{1 - \frac{2\upsilon}{\mu_1}, 1 - \zeta\}$. Thus, the proof is complete. □

**Lemma 2.** *Suppose that Assumptions A1 and A2 hold. Then, the following relations hold:*

$$a_{-1} = a_0, \quad a_{k+1} - a_k \leq \tau_k(a_k - a_{k-1}) + b_k - \gamma(2-\gamma)\frac{t_k^4\sigma^2\kappa_1^2\|d_k\|^4}{\|G(z_k)\|^2},$$

*where $a_k = \|x_k - x_*\|^2$ and $b_k = 2\tau_k\|x_k - x_{k-1}\|^2$.*

*Proof.* It is easy to see that $a_{-1} = a_0$ holds due to $x_{-1} = x_0$ and the definition of $a_k$. We begin by applying the adaptive line search in (2.12) and using the definition of $z_k$. This leads to the following:

$$G(z_k)^T(y_k - z_k) = -t_k G(z_k)^T d_k \geq t_k^2\sigma M_k(i_k)\|d_k\|^2 \geq t_k^2\sigma\kappa_1\|d_k\|^2 > 0, \tag{3.2}$$

which, together with Assumption A2, yields:

$$\begin{aligned} G(z_k)^T(y_k - x_*) &= G(z_k)^T(y_k - z_k) + G(z_k)^T(z_k - x_*) \\ &= G(z_k)^T(y_k - z_k) + (G(z_k) - G(x_*))^T(z_k - x_*) \\ &\geq G(z_k)^T(y_k - z_k). \end{aligned} \tag{3.3}$$

Using the projection operator $\mathcal{P}_{\mathcal{D}}[\cdot]$ and the non-expansive property in (2.14), we obtain:

$$\begin{aligned} \|x_{k+1} - x_*\|^2 &= \left\|\mathcal{P}_{\mathcal{D}}\left[y_k - \gamma\vartheta_k G(z_k)\right] - \mathcal{P}_{\mathcal{D}}\left[x_*\right]\right\|^2 \\ &\leq \|y_k - \gamma\vartheta_k G(z_k) - x_*\|^2 \\ &= \|y_k - x_*\|^2 - 2\gamma\vartheta_k G(z_k)^T (y_k - x_*) + \gamma^2\vartheta_k^2\|G(z_k)\|^2. \end{aligned}$$

Using the above inequality and (3.3), we obtain:

$$\|x_{k+1} - x_*\|^2 \leq \|y_k - x_*\|^2 - 2\gamma\vartheta_k G(z_k)^T (y_k - z_k) + \gamma^2\vartheta_k^2\|G(z_k)\|^2,$$

which, together with the definition of $\vartheta_k$ and (3.2), yields:

$$\begin{aligned} \|x_{k+1} - x_*\|^2 &\leq \|y_k - x_*\|^2 - \gamma(2-\gamma)\frac{\left(G(z_k)^T(y_k - z_k)\right)^2}{\|G(z_k)\|^2} \\ &\leq \|y_k - x_*\|^2 - \gamma(2-\gamma)\frac{t_k^4\sigma^2\kappa_1^2\|d_k\|^4}{\|G(z_k)\|^2}. \end{aligned} \tag{3.4}$$

Next, we analyze the term $\|y_k - x_*\|^2$. Using the definition of $y_k$, we get:

$$\begin{aligned} \|y_k - x_*\|^2 &= \|x_k + \tau_k(x_k - x_{k-1}) - x_*\|^2 \\ &= \|x_k - x_*\|^2 + \tau_k\left(x_k - x_{k-1}\right)^T\left(x_k - x_*\right) + \tau_k^2\left\|x_k - x_{k-1}\right\|^2 \\ &= \|x_k - x_*\|^2 + \tau_k\left(\|x_k - x_*\|^2 - \|x_{k-1} - x_*\|^2\right) + \left(\tau_k^2 + \tau_k\right)\|x_k - x_{k-1}\|^2. \end{aligned}$$

Considering the range of $\tau_k$ (i.e., $0 \leq \tau_k \leq 1$), we obtain:

$$\|y_k - x_*\|^2 \leq \|x_k - x_*\|^2 + \tau_k\left(\|x_k - x_*\|^2 - \|x_{k-1} - x_*\|^2\right) + 2\tau_k\left\|x_k - x_{k-1}\right\|^2. \tag{3.5}$$

Combining (3.4) with (3.5), we conclude that the proof is complete. □

**Lemma 3.** *Suppose that Assumptions A1 and A2 hold. Under these conditions, it follows that the limit* $\lim_{k\to+\infty}\|x_k - x_*\|$ *exists with* $x_* \in \mathcal{D}_*$.

*Proof.* From Lemma 2, together with the fact that $\gamma \in (0, 2)$, we have the relation $a_{k+1} - a_k \leq \tau_k(a_k - a_{k-1}) + b_k$. Applying this inequality, we obtain:

$$c_{k+1} \leq \tau_k c_k + b_k \leq \tau_k h(c_k) + b_k,$$

where $c_k := a_k - a_{k-1}$ and $h(\cdot) = \max\{\cdot, 0\}$. Using this inequality, and knowing that $\tau \in (0, 1)$ and $c_0 = 0$, we further derive:

$$h(c_{k+1}) \leq \tau_k h(c_k) + b_k \leq \tau^{k+1}h(c_0) + \sum_{i=0}^{k}\tau^i b_{k-i} = \sum_{i=0}^{k}\tau^i b_{k-i}.$$

Summing both sides of this inequality from 0 to $\infty$, we obtain:

$$\sum_{k=0}^{+\infty}h(c_{k+1}) \leq \sum_{k=0}^{+\infty}\left(\sum_{i=0}^{k}\tau^i b_{k-i}\right) \leq \sum_{k=0}^{+\infty}\left(\sum_{i=0}^{k}\tau^i b_k\right) \leq \sum_{k=0}^{+\infty}\left(\sum_{i=0}^{+\infty}\tau^i b_k\right).$$

This leads, in combination with (2.9), to:

$$\sum_{k=0}^{+\infty} h(c_{k+1}) \leq \left(\sum_{i=0}^{+\infty} \tau^i\right)\left(\sum_{k=0}^{+\infty} b_k\right) = \frac{1}{1-\tau}\sum_{k=0}^{+\infty} b_k < +\infty, \tag{3.6}$$

which implies that the sequence $\left\{\sum_{i=0}^{k} h(c_i)\right\}$ is bounded above. Let $e_k := a_k - \sum_{i=0}^{k} h(c_i)$, and we have from $a_k \geq 0$ that $\{e_k\}$ is bounded below. Moreover, we can further derive:

$$\begin{aligned} e_{k+1} &= a_{k+1} - h(c_{k+1}) - \sum_{i=0}^{k} h(c_i) \\ &\leq a_{k+1} - c_{k+1} - \sum_{i=0}^{k} h(c_i) \\ &= a_k - \sum_{i=0}^{k} h(c_i) \\ &= e_k. \end{aligned} \tag{3.7}$$

This infers that the sequence $\{e_k\}$ is non-increasing. Thus, the limit $\lim_{k\to+\infty} e_k$ exists, and from 3.7, we obtain:

$$\lim_{k\to+\infty} a_k = \lim_{k\to+\infty}\left(e_k + \sum_{i=0}^{k} h(c_i)\right) = \lim_{k\to+\infty} e_k + \sum_{i=0}^{\infty} h(c_i) < +\infty.$$

Hence, we conclude that the limit $\lim_{k\to+\infty} \|x_k - x_*\|$ exists. □

**Lemma 4.** *Suppose that Assumptions A1 and A2 hold. Under these conditions, it follows that the sequences* $\{x_k\}$ *and* $\{y_k\}$ *are both bounded.*

*Proof.* From Lemma 3, we know that the sequence $\{x_k\}$ is bounded. Furthermore, from (2.9), we deduce that $\lim_{k\to+\infty} \tau_k\|x_k - x_{k-1}\|^2 = 0$. Now, considering the definition of $y_k$ and the fact that $0 \leq \tau_k \leq \tau < 1$, we can derive the following:

$$\|y_k - x_k\|^2 = \tau_k^2\|x_k - x_{k-1}\|^2 \leq \tau_k\|x_k - x_{k-1}\|^2,$$

which leads to the conclusion:

$$\lim_{k\to+\infty} \|y_k - x_k\| = 0. \tag{3.8}$$

Thus, the sequence $\{y_k\}$ is also bounded.

□

**Lemma 5.** *For all* $k \geq 0$*, the search direction generated from* (2.10) *and* (2.11) *satisfies the trust region feature, i.e.,*

$$N\|G(y_k)\| \leq \|d_k\| \leq M\|G(y_k)\|, \tag{3.9}$$

*where* $M = \min\{1 + \frac{4}{\mu_2}, 1 + \zeta\}$.

*Proof.* We begin by considering the conjugate coefficient $\beta_k^{IHCGP}$, which, along with $0 < \lambda_k < 1$, can be simplified as:

$$\left|\beta_k^{IHCGP}\right| \leq \frac{2\left(\|G(y_k)\|^2 + \|G(y_k)\|^2\right)}{\mu_2\|G(y_k)\|\|d_{k-1}\|} = \frac{4}{\mu_2}\frac{\|G(y_K)\|}{\|d_{k-1}\|}. \tag{3.10}$$

We now proceed with the proof, considering two cases:

(i) If $-\upsilon_1\|G(y_{k-1})\|^2 \leq G(y_k)^T d_{k-1} \leq \upsilon_2\|G(y_{k-1})\|^2$, then, combining this with (2.10) and (3.10), we deduce the following inequality:

$$\begin{aligned} \|d_k\| &= \| - G(y_k) + \beta_k^{IHCGP} d_{k-1}\| \\ &\leq \|G(y_k)\| + \left|\beta_k^{IHCGP}\right| \|d_{k-1}\| \\ &\leq \|G(y_k)\| + \tfrac{4}{\mu_2}\tfrac{\|G(y_K)\|}{\|d_{k-1}\|}\|d_{k-1}\| \\ &\leq \left(1 + \tfrac{4}{\mu_2}\right)\|G(y_k)\|. \end{aligned}$$

(ii) If $G(y_k)^T d_{k-1} < -\upsilon_1\|G(y_{k-1})\|^2$ or $G(y_k)^T d_{k-1} > \upsilon_2\|G(y_{k-1})\|^2$, then, using (2.10), we obtain:

$$\|d_k\| \leq \|G(y_k)\| + \zeta\frac{\|G(y_k)\|\|d_{k-1}\|}{\|d_{k-1}\|^2}\|d_{k-1}\| \leq (1+\zeta)\,\|G(y_k)\|.$$

Thus, combining the results from these two cases, we conclude that:

$$\|d_k\| \leq M\|G(y_k)\|, \quad M = \min\left\{1 + \frac{4}{\mu_2}, 1 + \zeta\right\}.$$

Finally, applying the Cauchy-Schwarz inequality, we obtain from Lemma 1:

$$-\|G(y_k)\|\|d_k\| \leq G(y_k)^T d_k \leq -N\|G(y_k)\|^2,$$

which implies that $\|d_k\| \geq N\|G(y_k)\|$. Thus, the proof is complete.

□

**Lemma 6.** *Suppose that Assumptions A1 and A2 hold. Under these conditions, it follows that the limit* $\lim_{k\to+\infty} t_k\|d_k\| = 0$*, where the sequence* $\{d_k\}$ *is generated by the IHCGPB algorithm.*

*Proof.* From Lemma 4 and the continuity of $G(\cdot)$, without loss of generality, we know that there exists a constant $\phi_1$ such that the following relations hold:

$$\|y_k\| \leq \phi_1, \quad \|G(y_k)\| \leq \phi_1, \quad \forall k \geq 0. \tag{3.11}$$

This, along with Lemma 5, implies that $\|d_k\| \leq M\|G(y_k)\| \leq M\phi_1$, meaning the sequence $\{d_k\}$ is bounded. Next, considering the definition of $z_k = y_k + t_k d_k$, $t_k \in (0, \varsigma]$, and Lemma 4, we deduce that the sequence $z_k$ is also bounded. Similarly, by the continuity of $G(\cdot)$, there exists a constant $\phi_2$ such that the following relation holds:

$$\|G(z_k)\| \leq \phi_2, \quad \forall k \geq 0. \tag{3.12}$$

Now, using Lemma 2 and the fact that $\tau_k \leq \tau$, we obtain the following inequality:

$$\gamma(2-\gamma)\frac{t_k^4\sigma^2\kappa_1^2\|d_k\|^4}{\|G(z_k)\|^2} \leq a_k - a_{k+1} + \tau_k(a_k - a_{k-1}) + b_k \leq a_k - a_{k+1} + \tau h(c_k) + b_k.$$

Summing both sides of this inequality, and using (3.6) and (2.9), we obtain:

$$\gamma(2-\gamma)\sigma^2\kappa_1^2\sum_{k=0}^{+\infty}\frac{t_k^4\|d_k\|^4}{\|G(z_k)\|^2} \leq a_0 + \sum_{k=0}^{+\infty}\tau h(c_k) + \sum_{k=0}^{+\infty} b_k < +\infty,$$

which implies that

$$\lim_{k\to\infty} \frac{t_k^4\|d_k\|^4}{\|G(z_k)\|^2} = 0.$$

This result, together with (3.12), leads to the conclusion that $\lim_{k\to+\infty} t_k\|d_k\| = 0$. Thus, the proof is complete. □

**Theorem 1.** *Suppose that Assumptions A1 and A2 hold. Under these conditions, it follows that the sequences* $\{x_k\}$, $\{y_k\}$, *and* $\{z_k\}$ *converge to a solution of the CNME* (1.1).

*Proof.* We begin by proving that $\lim_{k\to+\infty} \inf \|G(y_k)\| = 0$. Assume that there exists a constant $\phi_3$ such that the following relation holds:

$$\|G(y_k)\| \le \phi_3, \quad \forall k \ge 0.$$

This result, combined with Lemma 5, implies that

$$\|d_k\| \ge N\|G(y_k)\| \ge N\phi_3. \tag{3.13}$$

Thus, applying Lemma 6, we obtain $\lim_{k\to\infty} t_k = 0$. Without loss of generality, from the boundedness of $\{y_k\}$ and $\{d_k\}$, we define the following limits:

$$\lim_{i\to+\infty} y_{k_i} = \ddot{y}, \quad \lim_{i\to+\infty} d_{k_i} = \ddot{d}.$$

Substituting $k := k_i$ into (3.1), we have $G(y_{k_i})^T d_{k_i} \le -N\|G(y_{k_i})\|^2$. Taking the limit in this inequality, and utilizing the continuity of $G(\cdot)$, we deduce:

$$G(\ddot{y})^T \ddot{d} \le -N\|G(\ddot{y})\|^2 < 0. \tag{3.14}$$

Furthermore, the step-length $\rho^{-1}t_k$ does not satisfy the adaptive line search in (2.12), i.e.,

$$-G(y_k + \rho^{-1}t_k d_k)^T d_k < \sigma\rho^{-1}t_k M_k(i_k)\|d_k\|^2 \le \sigma\rho^{-1}t_k\kappa_2\|d_k\|^2.$$

Substituting $k := k_i$ into the above inequality, we have $G(y_{k_i} + \rho^{-1}t_{k_i}d_{k_i})^T d_{k_i} > -\sigma\rho^{-1}t_{k_i}\kappa_2\|d_{k_i}\|^2$. Taking the limit in this inequality, and utilizing the continuity of $G(\cdot)$ and $\lim_{k\to\infty} t_k = 0$, we deduce:

$$G(\ddot{y})^T \ddot{d} \ge 0,$$

which contradicts (3.14). Thus, we conclude that $\lim_{k\to+\infty} \inf \|G(y_k)\| = 0$.

Next, from (3.11) and $\lim_{k\to+\infty} \inf \|G(y_k)\| = 0$, we defined the following limits:

$$\lim_{i\to+\infty} y_{k_i} = \ddot{y}, \quad \lim_{i\to+\infty} \|G(y_{k_i})\| = \|G(\ddot{y})\| = 0. \tag{3.15}$$

Note that from (3.8) and (3.15), it follows that $\lim_{i\to+\infty} x_{k_i} = \ddot{y}$. Since $x_{k_i} \in \mathcal{D}$ and $\mathcal{D}$ is a closed set, we conclude that $\ddot{y} \in \mathcal{D}$. Additionally, (3.15) shows that $\ddot{y} \in \mathcal{D}_*$. Using Lemma 3 for $x_* := \ddot{y}$ and $\lim_{i\to+\infty} x_{k_i} = \ddot{y}$, we obtain:

$$\lim_{k\to+\infty} \|x_k - \ddot{y}\| = \lim_{i\to+\infty} \|x_{k_i} - \ddot{y}\| = 0,$$

which implies that the sequence $\{x_k\}$ converges to $\ddot{y} \in \mathcal{D}_*$. Moreover, using the definition of $z_k$ and Lemma 6, we conclude that $\lim_{k\to+\infty} \|z_k - y_k\| = 0$. Combining this with (3.8), we conclude that both sequences $\{y_k\}$ and $\{z_k\}$ converge to $\ddot{y}$. Thus, the proof is complete. □

## 4. Numerical experiments

We conduct numerical experiments aimed at solving large-scale constrained nonlinear monotone equations as well as impulse noise image restoration problems. To evaluate the performance and competitiveness of the IHCGPB algorithm, we compare it with two existing methods: the CGAIS algorithm [26] and the JHCGPM algorithm [27]. The parameter settings for the IHCGPB algorithm are as follows:

$$\epsilon = 10^{-6},\ \mu_1 = 2,\ \mu_2 = 4,\ \tau = 0.015,\ \varsigma = 1,\ \rho = 0.55,\ \sigma = 0.0001,\ \kappa_1 = 0.001,$$
$$\kappa_2 = 0.8,\ \upsilon_1 = 0.9,\ \upsilon_2 = 0.4,\ \gamma = 1.55, \lambda_k = \left|G(y_k)^T d_{k-1}\right| / \|G(y_k)\|\,\|d_{k-1}\|.$$

The parameter settings for the CGAIS and JHCGPM algorithms are adopted directly from their respective original references. All three algorithms were executed on a Lenovo PC, which is equipped with a 2.10 GHz CPU, 16 GB RAM, and the Windows 11 operating system.

### *4.1. Constrained nonlinear monotone equations*

In the following, we consider a series of test problems where the function $G(x) = (G_1(x), G_2(x), \ldots, G_n(x))^T$ is defined for $x = (x_1, x_2, \ldots, x_n)$. These test problems are designed to assess the performance of the IHCGPB algorithm in solving large-scale constrained nonlinear monotone equations. For each of these problem, we select the initial points as follows: $x_1 = \left(\frac{1}{2}, \frac{1}{2^2}, \ldots, \frac{1}{2^n}\right)$, $x_2 = \left(0, \frac{1}{n}, \ldots, \frac{n-1}{n}\right)$, $x_3 = \left(1, \frac{1}{2}, \ldots, \frac{1}{n}\right)$, $x_4 = \left(\frac{1}{n}, \frac{2}{n}, \ldots, \frac{n}{n}\right)$, $x_5 = \left(\frac{n-1}{n}, \frac{n-2}{n}, \ldots, \frac{n-n}{n}\right)$, $x_6 = (1, 1, \ldots, 1)$, $x_7 = \left(\frac{1}{3}, \frac{1}{3^2}, \ldots, \frac{1}{3^n}\right)$, $x_8 = randn(n, 1)$. The dimension of each test problem is selected from the set $\{10000, 50000, 100000, 150000, 200000\}$. The specific problem formulations are outlined as follows:

**Problem 1.** The equations are given by:

$$\begin{aligned} G_1(x) &= e^{x_1} - 1, \\ G_i(x) &= e^{x_i} + x_i - 1, \quad \text{for } i = 2, 3, \ldots, n, \end{aligned}$$

and the domain remains $\mathcal{D} = \mathbb{R}^n_+$.

**Problem 2.** The equation is given by:

$$G_i(x) = e^{x_i} - 1, \quad \text{for } i = 1, 2, \ldots, n,$$

and the domain remains $\mathcal{D} = \mathbb{R}^n_+$.

**Problem 3.** The equations are given by:

$$\begin{aligned} G_1(x) &= 2x_1 + 0.5h^2(x_1 + h)^3 x_2, \\ G_i(x) &= 2x_i - x_{i-1} + x_{i+1} + 0.5h^2(x_i + ih)^3, \quad \text{for } i = 2, 3, \ldots, n-1, \\ G_n(x) &= 2x_n - x_{n-1} + 0.5h^2(x_n + nh)^3, \end{aligned}$$

and the domain remains $\mathcal{D} = \mathbb{R}^n_+$, $h = \frac{1}{n+1}$.

**Problem 4.** The equations are given by:

$$G_1(x) = x_1 - e^{\cos(\frac{x_1 + x_2}{2})},$$

$$\begin{aligned} G_i(x) &= x_i - e^{\cos(\frac{x_{i-1}+x_i+x_{i+1}}{i})}, \quad \text{for } i = 2, 3, \ldots, n-1, \\ G_n(x) &= x_n - e^{\cos(\frac{x_{n-1}+x_n}{n})}, \end{aligned}$$

and the domain remains $\mathcal{D} = \mathbb{R}^n_+$.

**Problem 5.** The equations are given by:

$$G_i(x) = \sqrt{8x_i} - 1, \quad \text{for } i = 1, 2, \ldots, n,$$

and the domain remains $\mathcal{D} = \mathbb{R}^n_+$.

**Problem 6.** The equations are given by:

$$\begin{aligned} G_1(x) &= x_1 + \sin(x_1) - 1, \\ G_i(x) &= -x_{i-1} + 2x_i + \sin(x_i) - 1, \quad \text{for } i = 2, 3, \ldots, n-1, \\ G_n(x) &= x_n + \sin(x_n) - 1, \end{aligned}$$

and the domain remains $\mathcal{D} = \{x \in \mathbb{R}^n : x \geq -3\}$.

**Problem 7.** The equations are given by:

$$G_i(x) = \ln(|x_i| + 1) - \frac{x_i}{n}, \quad \text{for } i = 1, 2, \ldots, n,$$

and the domain remains $\mathcal{D} = \mathbb{R}^n_+$.

**Problem 8.** The system is given by:

$$G_i(x) = x_i - \sin(|x_i - 1|), \quad \text{for } i = 1, 2, \cdots, n,$$

and the domain remains $\mathcal{D} = \mathbb{R}^n_+$.

The comparison results can be found at https://www.cnblogs.com/reports/p/18795260, where the term "IP" refers to the initial points, the term "Dim" refers to the dimension of the test problems, the term "RTim" refers to the running time in seconds, the term "NFun" refers to the number of function evaluations, the term "NIte" refers to the number of iterations, and the term "$G_*$" refers to the value of $\|G(x_k)\|$ when the code terminates. To effectively present the performance of the three algorithms, we utilize the performance profiles introduced by Dolan and Moré [28], which are defined as follows:

$$\rho(\tau) := \frac{1}{|T_P|} \left| \left\{ t_p \in T_P \mid \log_2 \left( \frac{t_{p,q}}{\min \left\{ t_{p,q} \mid q \in Q \right\}} \right) \leq \tau \right\} \right|,$$

where $T_P$ is the test problem set, $|T_P|$ is the number of problems in the set $T_P$, $Q$ is the set of optimization solvers, and $t_{p,q}$ is the number of iterations (or the number of function evaluations or running time in seconds) for $t_p \in T_P$ and $q \in Q$. These profiles provide a clear visual illustration of the numerical results. Specifically, Figures 1–3 display the performance of the algorithms in terms of NIte, NFun, and RTim. From these figures, it is evident that the IHCGPB algorithm outperforms both the CGAIS and JHCGPM algorithms. In general, the higher the curve of $\rho(\tau)$, the better the numerical performance of the corresponding method.

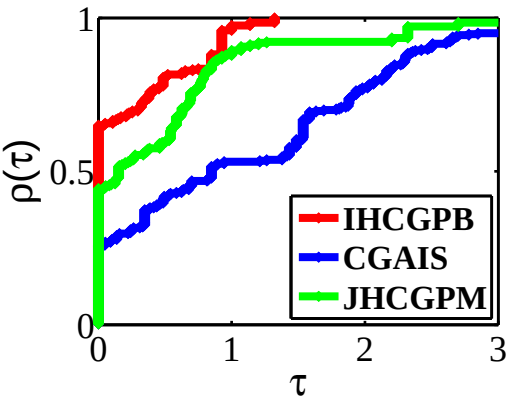


**Figure 1.** Performance profiles on NIte.

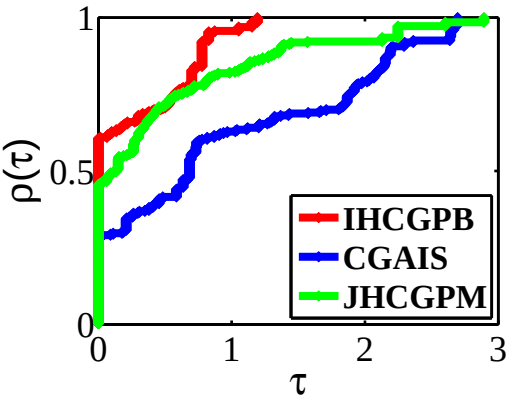


**Figure 2.** Performance profiles on NFun.

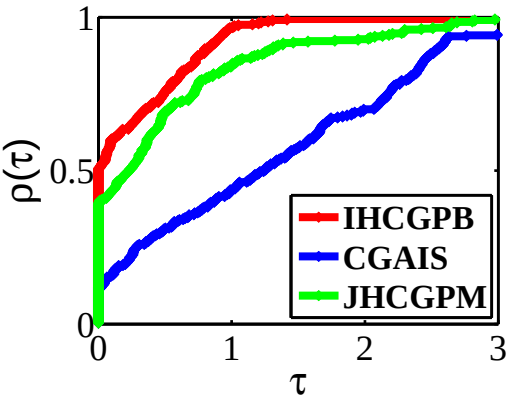


**Figure 3.** Performance profiles on RTim.

### 4.2. Application to impulse noise image restoration

The goal of impulse noise image restoration is to remove impulse noise (i.e., salt-and-pepper noise), which arises from faulty pixels in camera sensors or transmission errors through noisy channels. In works such as [29,30], a two-phase scheme is proposed for detecting and removing impulse noise. The first stage of the scheme involves using an adaptive median filter to identify noisy pixels, denoted by $\mathcal{I}$. Once the noisy pixels are detected, the second stage focuses on removing these noisy pixels by solving a smooth optimization problem. Specifically, the problem is formulated as:

$$\min f(x) := \sum_{(i,j)\in\mathcal{I}} 2\chi^1_{i,j} + \chi^2_{i,j},$$

where

$$\chi^1_{i,j} = \sum_{(m,n)\in\mathcal{J}_{i,j}\setminus\mathcal{I}} \psi_\alpha\left(x_{i,j} - y_{m,n}\right), \quad \chi^2_{i,j} = \sum_{(m,n)\in\mathcal{J}_{i,j}\cap\mathcal{I}} \psi_\alpha\left(x_{i,j} - x_{m,n}\right).$$

Here, $\mathcal{J}_{i,j}$ denotes the set of four neighbors at the pixel $(i, j)$, and $y_{m,m}$ represents the pixel value of the image at position $(m, n)$. The function $\psi_\alpha(\cdot)$ serves as an edge-preserving potential function. In particular, we adopt the Huber function as $\psi_\alpha(\cdot)$, which is defined as:

$$\psi_\alpha(o) = \begin{cases} \frac{o^2}{2\alpha}, & \text{if } |o| \le \alpha, \\ |o| - \frac{\alpha}{2}, & \text{otherwise.} \end{cases}$$

The Huber function is convex and first-order Lipschitz continuous, which ensures that the gradient $G(x) := \nabla f(x)$ is monotone. This property plays a crucial role in solving the optimization problem efficiently, as it guarantees the existence of a well-behaved solution.

In this experiment, we consider 24 grayscale test images, which are available at http://www.hlevkin.com. Each image is contaminated by 40% and 60% impulse noise, simulating an impulse noise image. For a fair comparison, the experiment is repeated 15 times with different noise samples, and the result are averaged. The experimental results are summarized in Table 1, where $\overline{NIte}$ and $\overline{RTim}$ denote the average number of iterations and average running time, respectively. To visually demonstrate the comparative results, we present a summary of the winners with respective to $\overline{NIte}$ and $\overline{RTim}$ in Table 2. The table indicates that the IHCGPB algorithm outperforms the other two algorithms in 79.17% (89.58%) of the cases for $\overline{NIte}$ ($\overline{RTim}$), while the other two algorithms win in 6.25% (2.08%) and 14.58% (8.33%) of the cases, respectively. Additionally, Figures 4 and 5 illustrate the restored images affected by 40% and 60% impulse noise, further highlighting the effectiveness of the proposed algorithm in image denoising.

**Table 1.** The numerical results for restoring impulse noise images.

| Image | Impulse | IHCGPB $\overline{NIte}/\overline{RTim}$ | CGAIS $\overline{NIte}/\overline{RTim}$ | JHCGPM $\overline{NIte}/\overline{RTim}$ |
|---|---|---|---|---|
| airplane(512×512) | 40% | 6.000/2.039 | 37.300/12.874 | 35.400/10.882 |
| | 60% | 23.100/7.550 | 45.000/20.495 | 47.000/16.863 |
| airplaneU2(1024×1024) | 40% | 14.000/16.232 | 16.400/30.794 | 13.600/18.639 |
| | 60% | 11.000/14.432 | 26.300/48.026 | 24.700/33.267 |

*Continued on the next page*

| Image | Impulse | IHCGPB $\overline{NIte}/\overline{RTim}$ | CGAIS $\overline{NIte}/\overline{RTim}$ | JHCGPM $\overline{NIte}/\overline{RTim}$ |
|---|---|---|---|---|
| brickwall(1024×1024) | 40% | 6.000/8.097 | 18.500/34.984 | 18.600/24.832 |
| | 60% | 18.000/22.032 | 29.400/53.224 | 25.600/36.406 |
| bridge(512×512) | 40% | 11.100/3.127 | 31.700/11.842 | 48.400/13.431 |
| | 60% | 9.800/4.096 | 39.100/18.824 | 39.700/15.622 |
| cameraman(256×256) | 40% | 8.300/0.419 | 51.500/3.821 | 35.000/2.306 |
| | 60% | 6.200/0.348 | 57.800/5.007 | 67.000/4.478 |
| carpet(1024×1024) | 40% | 28.600/27.781 | 28.000/42.793 | 17.400/24.354 |
| | 60% | 37.400/38.786 | 39.500/63.037 | 65.900/90.172 |
| clown(512×512) | 40% | 7.000/2.404 | 38.300/13.687 | 27.300/8.419 |
| | 60% | 12.000/4.685 | 40.500/20.458 | 37.600/14.450 |
| couple(512×512) | 40% | 7.100/2.427 | 32.400/12.082 | 39.300/12.371 |
| | 60% | 6.000/3.031 | 35.600/17.670 | 31.800/12.439 |
| crowd(512×512) | 40% | 7.000/2.176 | 26.300/9.636 | 22.200/7.373 |
| | 60% | 6.000/3.003 | 38.700/18.712 | 35.300/13.842 |
| finger(256×256) | 40% | 28.800/1.339 | 24.900/2.009 | 8.500/0.427 |
| | 60% | 26.200/1.279 | 43.700/3.504 | 9.100/0.481 |
| girlface(512×512) | 40% | 17.700/4.667 | 36.500/13.851 | 18.800/5.749 |
| | 60% | 14.400/5.894 | 24.900/12.519 | 22.600/9.499 |
| houses(512×512) | 40% | 106.800/22.607 | 45.600/15.660 | 67.500/20.086 |
| | 60% | 132.400/35.606 | 62.400/28.365 | 47.700/17.925 |
| kiel(512×512) | 40% | 11.000/3.025 | 45.500/15.567 | 31.200/10.167 |
| | 60% | 8.000/3.640 | 65.700/31.913 | 51.400/19.311 |
| lighthouse(512×512) | 40% | 11.900/3.285 | 41.000/13.657 | 22.400/7.894 |
| | 60% | 7.800/3.601 | 49.900/24.292 | 54.000/20.492 |
| lungs(425×425) | 40% | 12.700/2.593 | 18.700/5.411 | 14.600/3.214 |
| | 60% | 10.300/2.616 | 20.800/6.144 | 20.100/4.507 |
| man(1024×1024) | 40% | 19.000/21.379 | 30.300/52.272 | 19.700/27.011 |
| | 60% | 17.000/20.465 | 38.700/66.013 | 24.700/33.600 |
| pepper(512×512) | 40% | 6.000/2.314 | 28.800/11.179 | 12.500/4.191 |
| | 60% | 20.000/7.182 | 48.300/22.125 | 34.300/13.320 |
| sailboat(512×512) | 40% | 7.000/2.426 | 31.200/11.593 | 34.800/11.655 |
| | 60% | 6.000/2.962 | 52.300/24.292 | 30.700/11.943 |
| tank(512×512) | 40% | 20.800/5.355 | 19.500/8.163 | 20.800/6.763 |
| | 60% | 9.900/4.167 | 24.000/12.654 | 26.300/10.393 |
| tank2(512×512) | 40% | 22.500/5.883 | 21.100/8.899 | 19.500/6.305 |
| | 60% | 14.000/5.373 | 32.300/15.700 | 27.600/10.825 |
| tiffany(512×512) | 40% | 9.500/3.072 | 29.700/12.152 | 20.100/6.423 |
| | 60% | 17.000/6.333 | 39.600/19.433 | 25.300/10.035 |
| truck(512×512) | 40% | 20.900/5.566 | 22.600/8.941 | 17.500/5.758 |
| | 60% | 14.000/5.470 | 29.600/14.293 | 25.100/9.965 |

*Continued on the next page*

| Image | Impulse | IHCGPB $\overline{NIte}/\overline{RTim}$ | CGAIS $\overline{NIte}/\overline{RTim}$ | JHCGPM $\overline{NIte}/\overline{RTim}$ |
|---|---|---|---|---|
| trucks(512×512) | 40% | 6.600/2.376 | 19.800/8.502 | 25.200/8.312 |
| | 60% | 13.800/5.278 | 29.600/13.770 | 30.800/11.196 |
| zelda(512×512) | 40% | 21.200/5.549 | 21.000/8.237 | 21.800/6.975 |
| | 60% | 6.000/3.348 | 29.100/13.455 | 25.800/9.719 |

**Table 2.** Winners with respect to $\overline{NIte}$ and $\overline{RTim}$.

| | IHCGPB | CGAIS | JHCGPM |
|---|---|---|---|
| | NW/Percentage(%) | NW/Percentage(%) | NW/Percentage(%) |
| $\overline{NIte}$ | 38/79.17% | 3/6.25% | 7/14.58% |
| $\overline{RTim}$ | 43/89.58% | 1/2.08% | 4/8.33% |

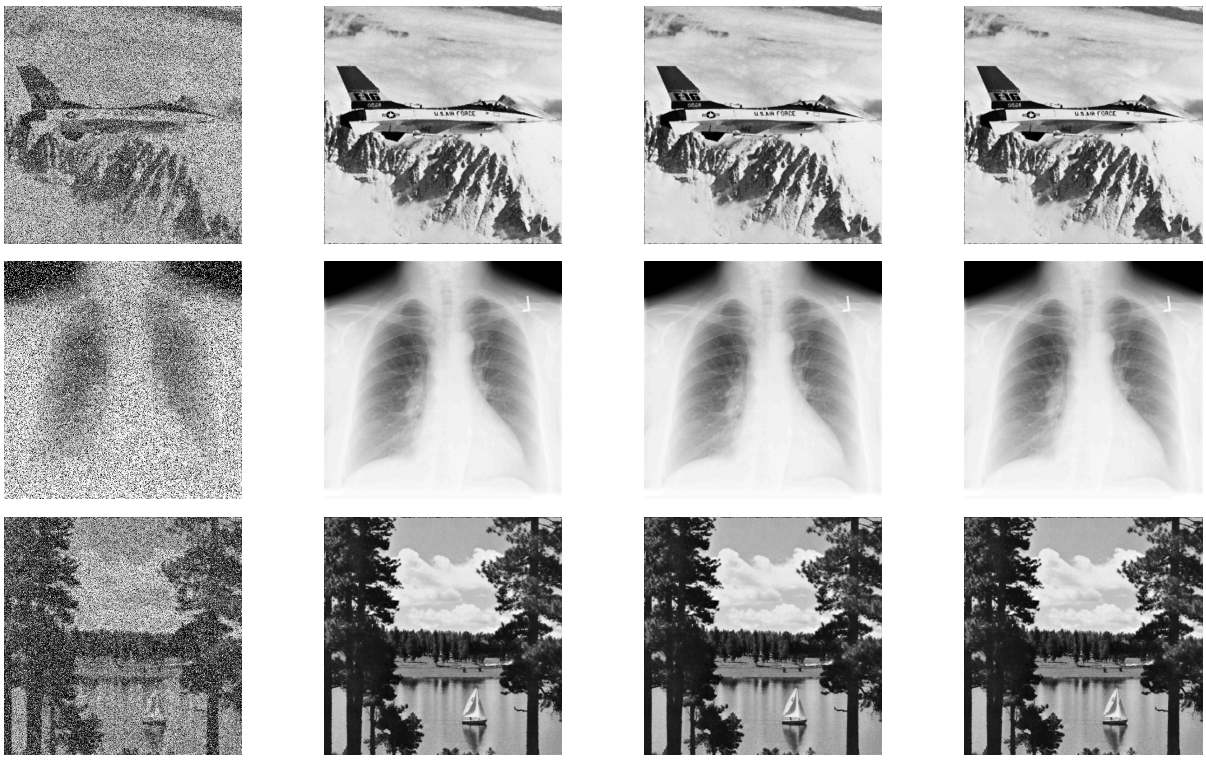

**Figure 4.** From left to right: an image with 40% impulse noise and restored images from the IHCGPB, CGAIS, and JHCGPM algorithms.

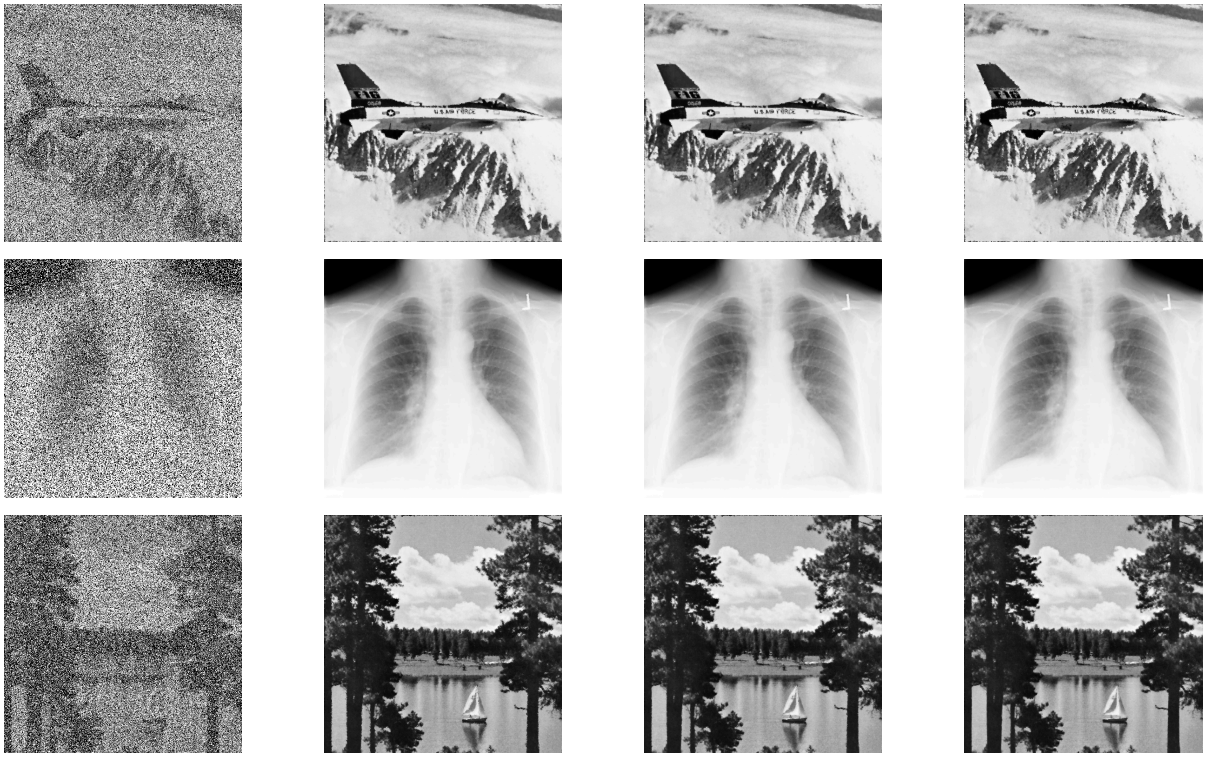

**Figure 5.** From left to right: an image with 60% impulse noise and restored images from the IHCGPB, CGAIS, and JHCGPM algorithms.

## 5. Conclusions

In this paper, we design a novel hybrid conjugate coefficient, which integrates the improved HS and PRP conjugate coefficients into a single parameter. This new coefficient is used to construct a search direction that satisfies both the sufficient descent property and the trust-region feature by introducing a restart strategy. Additionally, we develop an inertial hybrid CGP-based algorithm by combining an inertial-related scheme with a projection technique, designed to address large-scale constrained nonlinear equations and impulse noise image restoration problems. The theoretical analysis of the proposed algorithm is performed under weaker assumptions, and its convergence is rigorously proved. Numerical experiments on large-scale constrained nonlinear equations and impulse noise image restoration demonstrate the superior numerical efficiency of the proposed algorithm compared to existing alternatives. Future work will focus on further improving the algorithm's performance, especially in more complex settings, and exploring its applicability to other types of optimization problems.

## Author contributions

Yan Xia: Conceptualization, Investigation, Writing–original draft, Funding acquisition; Dandan Li: Investigation, Writing–review and editing. All authors have read and approved the final version of the manuscript for publication.

## Use of Generative-AI tools declaration

The authors declare they have not used Artificial Intelligence (AI) tools in the creation of this article.

## Acknowledgments

This research was funded by the Guangzhou Huashang College Daoshi Project (No. 2024HSDS28).

## Conflict of interest

The authors declare that there are no conflicts of interest regarding the publication of this paper.

## References

1. G. Ma, J. Jin, J. Jian, J. Yin, D. Han, A modified inertial three-term conjugate gradient projection method for constrained nonlinear equations with applications in compressed sensing, *Numer. Algor.*, **92** (2023), 1621–1653. https://doi.org/10.1007/s11075-022-01356-1
2. M. Koorapetse, P. Kaelo, S. Lekoko, T. Diphofu, A derivative-free RMIL conjugate gradient projection method for convex constrained nonlinear monotone equations with applications in compressive sensing, *Appl. Numer. Math.*, **165** (2021), 431–441. https://doi.org/10.1016/j.apnum.2021.03.005
3. X.-B. Jin, X.-Y. Zhang, K. Huang, G.-G. Geng, Stochastic conjugate gradient algorithm with variance reduction, *IEEE Trans. Neur. Net. Learn. Syst.*, **30** (2019), 1360–1369. https://doi.org/10.1109/TNNLS.2018.2868835
4. A. B. Abubakar, A. H. Ibrahim, Y. Feng, Derivative-free projection CG-based algorithm with restart strategy for solving convex-constrained nonlinear monotone equations and its application to logistic regression, *J. Comput. Appl. Math.*, **471** (2026), 116676. https://doi.org/10.1016/j.cam.2025.116676
5. P. Liu, L. Li, H. Shao, M. Liu, J. Fan, An inertial-type CG projection method with restart for pseudo-monotone costs with application to traffic assignment, *Netw. Spat. Econ.*, **25** (2025), 147–172. https://doi.org/10.1007/s11067-024-09653-z
6. G. Zhou, K. Toh, Superlinear convergence of a Newton-type algorithm for monotone equations, *J. Optim. Theory Appl.*, **125** (2005), 205–221. https://doi.org/10.1007/s10957-004-1721-7
7. B. Polyak, A. Tremba, New versions of Newton method: step-size choice, convergence domain and under-determined equations, *Optim. Method. Softw.*, **35** (2020), 1272–1303. https://doi.org/10.1080/10556788.2019.1669154
8. Z. Chen, W. Cheng, X. Li, A global convergent quasi-Newton method for systems of monotone equations, *J. Appl. Math. Comput.*, **44** (2014), 455–465. https://doi.org/10.1007/s12190-013-0702-0
9. C. A. Arias, C. Gómez, Inexact free derivative quasi-Newton method for large-scale nonlinear system of equations, *Numer. Algor.*, **94** (2023), 1103–1123. https://doi.org/10.1007/s11075-023-01529-6

10. J. Yin, J. Jian, G. Ma, A modified inexact Levenberg-Marquardt method with the descent property for solving nonlinear equations, *Comput. Optim. Appl.*, **87** (2024), 289–322. https://doi.org/10.1007/s10589-023-00513-z

11. S. B. Salihu, A. S. Halilu, M. Abdullahi, K. Ahmed, P. Mehta, S. Murtala, An improved spectral conjugate gradient projection method for monotone nonlinear equations with application, *J. Appl. Math. Comput.*, **70** (2024), 3879–3915. https://doi.org/10.1007/s12190-024-02121-4

12. M. Y. Waziri, K. Ahmed, A. S. Halilu, A modified PRP-type conjugate gradient projection algorithm for solving large-scale monotone nonlinear equations with convex constraint, *J. Comput. Appl. Math.*, **407** (2022), 114035. https://doi.org/10.1016/j.cam.2021.114035

13. J. Yin, J. Jian, X. Jiang, M. Liu, L. Wang, A hybrid three-term conjugate gradient projection method for constrained nonlinear monotone equations with applications, *Numer. Algor.*, **88** (2021), 389–418. https://doi.org/10.1007/s11075-020-01043-z

14. D. Li, S. Wang, Y. Li, J. Wu, A convergence analysis of hybrid gradient projection algorithm for constrained nonlinear equations with applications in compressed sensing, *Numer. Algor.*, **95** (2024), 1325–1345. https://doi.org/10.1007/s11075-023-01610-0

15. D. Li, S. Wang, Y. Li, J. Wu, A modified SGP method with two alternative spectral parameters for constrained nonlinear equations with a compressive sensing application, *J. Comput. Appl. Math.*, **463** (2025), 116503. https://doi.org/10.1016/j.cam.2025.116503

16. P. Liu, H. Shao, Z. Yuan, X. Wu, T. Zheng, A family of three-term conjugate gradient projection methods with a restart procedure and their relaxed-inertial extensions for the constrained nonlinear pseudo-monotone equations with applications, *Numer. Algor.*, **94** (2023), 1055–1083. https://doi.org/10.1007/s11075-023-01527-8

17. W. Liu, J. Jian, J. Yin, An inertial spectral conjugate gradient projection method for constrained nonlinear pseudo-monotone equations, *Numer. Algor.*, **97** (2024), 985–1015. https://doi.org/10.1007/s11075-023-01736-1

18. H. Zheng, J. Li, P. Liu, X. Rong, An inertial Fletcher-Reeves-type conjugate gradient projection-based method and its spectral extension for constrained nonlinear equations, *J. Appl. Math. Comput.*, **70** (2024), 2427–2452. https://doi.org/10.1007/s12190-024-02062-y

19. P. Liu, H. Shao, Z. Yuan, J. Zhou, A family of inertial-based derivative-free projection methods with a correction step for constrained nonlinear equations and their applications, *Numer. Linear Algebra Appl.*, **31** (2024), e2533. https://doi.org/10.1002/nla.2533

20. N. Zhang, J. K. Liu, L. Q. Zhang, Z. L. Lu, A fast inertial self-adaptive projection based algorithm for solving large-scale nonlinear monotone equations, *J. Comput. Appl. Math.*, **426** (2023), 115087. https://doi.org/10.1016/j.cam.2023.115087

21. A. H. Ibrahim, S. Al-Homidan, Two-step inertial derivative-free projection method for solving nonlinear equations with application, *J. Comput. Appl. Math.*, **451** (2024), 116071. https://doi.org/10.1016/j.cam.2024.116071

22. J. L. Nazareth, Conjugate-gradient methods, In: *Encyclopedia of optimization*, Boston: Springer, 2008, 466–470. https://doi.org/10.1007/978-0-387-74759-0_85

23. Z. Wei, H. Huang, Y. Tao, A modified Hestenes-Stiefel conjugate gradient method and its convergence, *J. Math. Res. Expos.*, **30** (2010), 297–308.

24. Y. Zhang, H. Zheng, C. Zhang, Global convergence of a modified PRP conjugate gradient method, *Procedia Engineering*, **31** (2012), 986–995. https://doi.org/10.1016/j.proeng.2012.01.1131

25. D. Li, J. Wu, Y. Li, S. Wang, A modified spectral gradient projection-based algorithm for large-scale constrained nonlinear equations with applications in compressive sensing, *J. Comput. Appl. Math.*, **424** (2023), 115006. https://doi.org/10.1016/j.cam.2022.115006

26. A. B. Muhammad, C. Tammer, A. M. Awwal, R. Elster, Z. Ma, Inertial-type projetion methods for sovling convex constrained monotone nonlinear equations with applications to robotic motion control, *J. Nonlinear Var. Anal.*, **5** (2021), 831–849. https://doi.org/10.23952/jnva.5.2021.5.13

27. X. Jiang, Z. Huang, An accelerated relaxed-inertial strategy based CGP algorithm with restart technique for constrained nonlinear pseudo-monotone equations to image de-blurring problems, *J. Comput. Appl. Math.*, **447** (2024), 115887. https://doi.org/10.1016/j.cam.2024.115887

28. E. D. Dolan, J. J. Moré, Benchmarking optimization software with performance profiles, *Math. Program.*, **91** (2002), 201–213. https://doi.org/10.1007/s101070100263

29. R. H. Chan, C. W. Ho, M. Nikolova, Salt-and-pepper noise removal by median-type noise detectors and detail-preserving regularization, *IEEE Trans. Image Process.*, **14** (2005), 1479–1485. https://doi.org/10.1109/TIP.2005.852196

30. J. F. Cai, R. H. Chan, C. Di Fiore, Minimization of a detail-preserving regularization functional for impulse noise removal, *J. Math. Imaging Vis.*, **29** (2007), 79–91. https://doi.org/10.1007/s10851-007-0027-4


AIMS Press